Passive time-domain numerical models of viscothermal wave propagation in acoustic tubes of variable cross section

Passive time-domain numerical models of viscothermal wave propagation in acoustic tubes of variable cross section

Stefan Bilbao[a] and Reginald Harrison
Acoustics and Audio Group, University of Edinburgh, James Clerk Maxwell Building, EH9 3JZ, Edinburgh, United Kingdom

(Received 15 April 2016; revised 21 June 2016; accepted 29 June 2016; published online 29 July 2016)

Numerical modeling of wave propagation in acoustic tubes is a subject of longstanding interest, particularly for enclosures of varying cross section, and especially when viscothermal losses due to boundary layer effects are taken into consideration. Though steady-state, or frequency domain methods, are a common avenue of approach, recursive time domain methods are an alternative, allowing for the generation of wideband responses, and offer a point of departure for more general modeling of nonlinear wave propagation. The design of time-domain methods is complicated by numerical stability considerations, and to this end, a passive representation is a useful design principle leading to simple stable and explicit numerical schemes, particularly in the case of viscothermal loss modeling. Such schemes and the accompanying energy and stability analysis are presented here. Numerical examples are presented for a variety of duct profiles, illustrating strict energy dissipation, and for comparison of computed input impedances against frequency-domain results.
 [http://dx.doi.org/10.1121/1.4959025]

[TRM] Pages: 728–740

I. INTRODUCTION

Numerical modeling of wave propagation in acoustic tubes is a subject of general interest. The focus of this article is on linear propagation in tubes of variable circular cross section, including boundary layer losses, according to the model of Zwikker and Kosten;[1] see the early review article by Tijdeman,[2] for a historical survey. As such models are usually expressed in terms of acoustic impedance and admittance, frequency domain approximation methods are a natural choice. For tubes of varying cross section, transmission matrix methods are commonly employed: for a fixed frequency, the differential equation corresponding to the acoustic tube is numerically integrated spatially, to yield, typically, a value of input impedance at that frequency. Various references cover the details of such methods.[3]

Time domain methods are another avenue of approach. In this case, the dynamical system corresponding to the tube is numerically integrated using a time-stepping method of some form. The advantages are, relative to frequency domain methods, that one may obtain wideband information through a directly calculated impulse response, and the possibility of generalizations to the case of nonlinear wave propagation, which is of particular interest in the acoustics of brass instruments[4] as well as to time-varying systems, such as the vocal tract.[5] Neither generalization is easily approached in a frequency-domain framework. The disadvantages are the need for control over numerical stability, and also the appearance of artifacts due to numerical truncation error. Though both difficulties are present as well in the case of frequency domain methods, they are a far more serious concern in the time domain case.

Time domain method design is often approached using a methodology based on the concatenation of tubes of simple profiles, such as cylinders or cones[6–8] or other types,[9] following from early work in vocal tract modeling.[10] Another approach is to make use of full time/space integration techniques, such as the finite difference time domain (FDTD) method[11] or finite volume method.[5] In this case, the tube is viewed as a unit, and the state is approximated over a spatial grid, assumed uniform in the case of FDTD. There are many possible designs, which differ considerably in terms of accuracy and stability properties.

One useful attribute of the underlying system such as an acoustic tube is that of an energy balance: the rate of change of the stored energy in the acoustic tube is equal to power input less the dissipated power; furthermore, the stored energy, a non-negative function of the state, serves as a Lyapunov function. In a discrete setting, such a balance can be built directly into a simulation algorithm, leading, ultimately, to a means of determining numerical stability conditions. Such methods fall under the umbrella of geometric or structure-preserving integration techniques, dealt with in detail in the case of lossless ordinary differential equations by Hairer and Wanner,[12] and by various authors in the present case of partial differential equations for systems in acoustics.[13,14] For the Zwikker-Kosten model, the use of such methods is complicated somewhat by the need for a passive finite-order approximation to the viscothermal immittances; one such approximation has been presented recently by Thompson *et al.*,[15] and another, suitable for optimization, by the present authors.[16] In this article, such approximations are used to design an energy-balanced time-stepping method, and to derive numerical stability conditions.

In Sec. II, a model of viscothermal wave propagation in a tube of variable cross section is presented, as well as approximations of varying degree to the boundary layer losses,

[a]Electronic mail: sbilbao@staffmail.ed.ac.uk

expressed in terms of a circuit representation. A time domain system results, possessing an energy balance, as is explicitly illustrated. Such a model has appeared recently in Ref. 16 and is included here for completeness. The basic machinery of finite difference time domain methods, including the definitions of grid functions and discrete operators appear in Sec. III, and a comparison of two distinct energy-conserving schemes for the simple case of the lossless cylinder is provided in Sec. IV. A discrete energy-balanced and explicit scheme for the full viscothermal system is presented in Sec. V, accompanied by energy-based stability analysis, leading to convenient stability conditions. Some numerical examples for various types of tube profile are presented in Sec. VI.

II. MODEL EQUATIONS

Consider an acoustic tube, aligned with the x axis, and of variable (circular) cross-sectional area $S(x)$, for $x \in \mathcal{D} = [0, L]$, where L is the tube length (see Fig. 1).

A frequency domain description of wave propagation in the tube[3] may be given as

$$\partial_x P + ZV = 0, \quad \partial_x (SV) + YSP = 0. \tag{1}$$

Here, $P = P(\omega, x)$ represents the acoustic pressure, and $V = V(\omega, x)$ the particle velocity, and ∂_x represents partial differentiation with respect to the spatial coordinate x. Such a one-dimensional model is valid for wavelengths which are long relative to the tube's lateral dimension.[17] Wavefronts are assumed planar in this study.

The expressions $Z = Z(\omega, x)$ and $Y = Y(\omega, x)$ represent the specific series impedance and shunt admittance per unit length, respectively, for the tube at coordinate x. Standard forms[3] for Z and Y are

$$Z = \frac{j\omega\rho}{1 - F_v}, \quad Y = \frac{j\omega}{\rho c^2}(1 + (\gamma - 1)F_\theta). \tag{2}$$

Here, c is the wave speed in m/s, ρ is air density, in kg/m^3, and γ is the ideal gas constant. The functions F_v and F_θ are defined by

$$F_v = \phi\left(\sqrt{-j}r_v\right), \quad F_\theta = \phi\left(\sqrt{-j}r_\theta\right), \quad \phi(\zeta) = \frac{2J_1(\zeta)}{\zeta J_0(\zeta)}. \tag{3}$$

Here J_0 and J_1 are zeroth and first order Bessel functions, $j = \sqrt{-1}$, and the nondimensional viscous/thermal boundary layer thicknesses r_v and r_θ are defined as

FIG. 1. An acoustic tube, aligned with a coordinate x, and with planar circular cross section $S(x)$.

$$r_v = \sqrt{S\rho\omega/\pi\eta}, \quad r_\theta = \sqrt{S\rho C_p\omega/\pi\kappa}, \tag{4}$$

where η is the viscosity coefficient, C_p the specific heat at constant pressure and κ the thermal conductivity. All thermodynamic constants, as well as wave speed and density exhibit a weak dependence on temperature; henceforth, in this article, they are set to values corresponding to a temperature of 26.85 °C, using formulae given by Benade.[18] The expressions in (3) above pertain to a tube of circular cross section; similar forms are available for tubes of other types of cross section (such as rectangular) and have little impact on the numerical construction techniques described in this article.

One boundary condition is required at either end of the domain. In this article, where the focus is on numerical modeling over the problem interior, the choices

$$V(\omega, 0) = V_{in}(\omega), \quad P(\omega, L) = 0, \tag{5}$$

correspond to a velocity-driven source at $x = 0$ and a crude approximation to an open tube end at $x = L$; far more refined models of radiation at the open end of a tube are available.[19] Such a condition is useful in the characterization of a tube in terms of its input impedance.

The model given in (1) is an extension to the case of a tube of variable cross section of that given for a cylindrical tube some time ago,[1] and is identical in form to that given by Caussé *et al.*[3]

A. Splitting of immittances

It is useful to split the immittances Z and Y as

$$Z = Z_l + Z_v, \quad Y = Y_l + Y_\theta. \tag{6}$$

Here, $Z_l = j\omega\rho$ and $Y_l = j\omega/\rho c^2$ are purely reactive immittances leading, in isolation, to lossless wave propagation. The immittances Z_v and Y_θ are defined as

$$Z_v = j\omega\rho\frac{F_v}{1 - F_v}, \quad Y_\theta = \frac{j\omega}{\rho c^2}(\gamma - 1)F_\theta, \tag{7}$$

and represent the effects of viscosity and heat transfer, respectively. System (1) can then be rewritten as

$$\begin{aligned} &\partial_x P + j\omega\rho V + Z_v V = 0, \\ &\partial_x (SV) + \frac{j\omega S}{\rho c^2} P + SY_\theta P = 0. \end{aligned} \tag{8}$$

When $Z_v = Y_\theta = 0$, system (1) reduces to

$$\partial_x P + j\omega\rho V = 0, \quad \partial_x (SV) + \frac{j\omega}{\rho c^2} SP = 0, \tag{9}$$

which can be reduced to a single second-order equation in P (Webster's equation,[20] in the frequency domain).

B. Positive realness and pole/zero distributions of immittances

The immittances Z_v and Y_θ correspond to viscous and thermal losses, respectively, in the tube. See Fig. 2 which

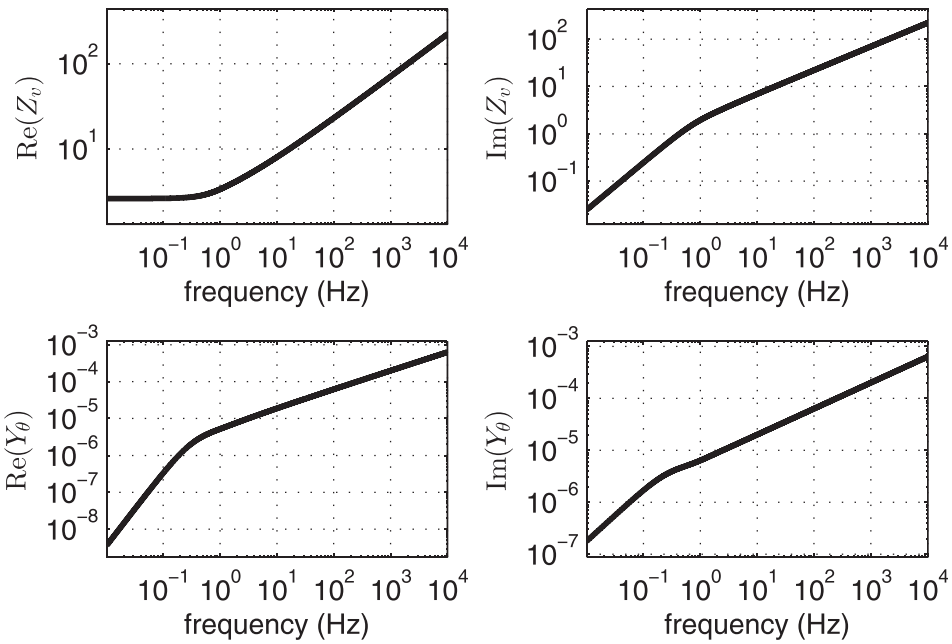

FIG. 2. Real and imaginary parts of Z_v, in $\mathrm{kg\,s^{-1}\,m^{-5}}$ and Y_θ, in $\mathrm{kg^{-1}\,s\,m^5}$, for a tube of radius 7.5 mm, at a temperature of 26.85 °C.

illustrates the frequency dependence of the real and imaginary parts of Z_v and Y_θ. As such, they are passive, and thus, under an extension to the complex plane using $j\omega \to s$, for a complex frequency variable s, they are positive real functions[21] (of infinite order). Both, however, are of a special form: the poles and zeros interlace along the negative real axis, with a zero nearest the origin in both cases (see Fig. 3). The immittances are reactive, implying, beyond dissipation, an energy storage mechanism (see Sec. II F).

C. Rational approximations and circuit representations

In order to arrive at a time domain model operating as a recursion, the immittances Z_v and Y_θ must necessarily be approximated. A common approach is to make use of a high-frequency approximation to Z_v and Y_θ in fractional powers of the frequency variable,[3,22] leading to a fractional-order differential equation. See, e.g., work on the Webster Lokshin model,[9,23] which derives from such an approximation under various simplifications. One difficulty is that the high-frequency approximation is not smooth in the low-frequency limit. Another approach is to develop rational approximants to the immittances directly—indeed, both are smooth functions in the limit of $s \to 0$. Such an approach leads naturally to circuit representations,[15,24] which may be truncated to finite order in preparation for a numerical design.

The interlacing of the poles and zeros of Z_v and Y_θ implies that either may be represented as a one-port with circuit elements of only two types (resistive/inductive, for Z_v and resistive/capacitive, for Y_θ). Canonical designs are available in this case, where all element values are non-negative, enforcing passivity. In particular, a continued fraction expansion leads to a Cauer structure for both immittances.[15] Approximation error decreases with truncation order, but convergence can be slow, requiring a large number of elements. This is an important consideration in a time domain implementation, as the order of the approximation to viscothermal losses is a bottleneck in terms of computational costs.

Alternatively, a Foster structure[25] results from partial fraction expansions and has been explored in recent work.[16] To this end, it is useful to decompose Y_θ as a series combination of a capacitor, of capacitance $C_0 = (\gamma - 1)/\rho c^2$, and an admittance $\tilde{Y}_\theta$, given by

$$\tilde{Y}_\theta = \frac{j\omega(\gamma - 1)}{\rho c^2} \frac{F_\theta}{1 - F_\theta}. \tag{10}$$

Now, the forms of Z_v, from (7) and $\tilde{Y}_\theta$ are the same, and thus the circuit structures are dual (see Fig. 4). When truncated to Mth order,

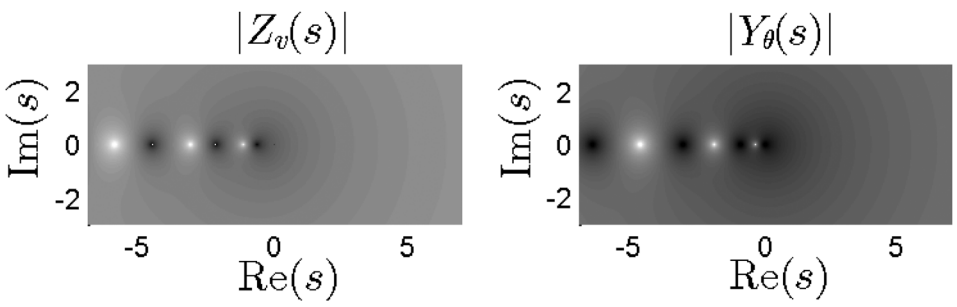

FIG. 3. Magnitude of (left) the series admittance $|Z_v(s)|$ and (right) shunt admittance $|Y_\theta(s)|$, in the complex plane, in dB. Zeros and poles appear as dark and light spots, respectively.

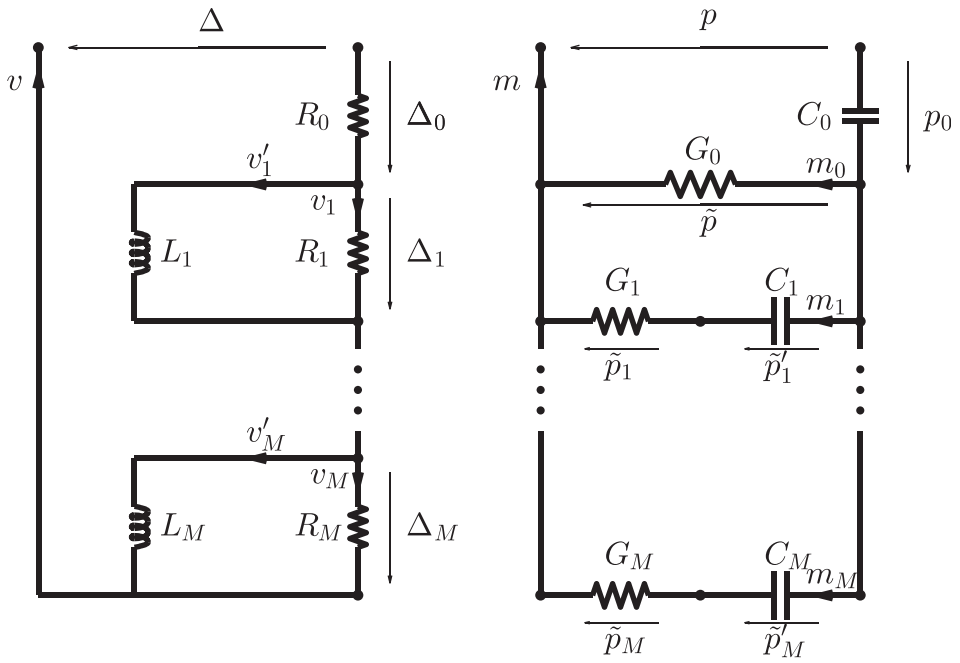

FIG. 4. M-branch Foster structures approximating (left) the impedance Z_v and (right) the admittance Y_θ (after the initial extraction of a capacitance).

$$Z_v^M = R_0 + \sum_{q=1}^{M} \frac{R_q L_q j\omega}{R_q + L_q j\omega},$$
$$\tilde{Y}_\theta^M = G_0 + \sum_{q=1}^{M} \frac{G_q C_q j\omega}{G_q + C_q j\omega}, \tag{11}$$

where Z_v^M and $\tilde{Y}_\theta^M$ are Mth order approximations to Z_v and $\tilde{Y}_\theta$, respectively. The immittances are parameterized by resistances R_q and conductances G_q, $q = 0, \ldots, M$, and inductances L_q and capacitances C_q, $q = 1, \ldots, M$. For passivity, all element values must be non-negative.

D. Optimization

Instead of deriving the element values from partial fraction expansions of the immittances, the forms in (11) above may be used as the starting point for optimization procedures. As recently shown,[16] excellent accuracy can be obtained over a wide frequency range using a relatively low number M of branches. The additive composition of the Foster structure allows for the use of simple optimization procedures, such as gradient descent.

In Fig. 5, fractional errors in the real part of the approximations Z_v^M to Z_v and are plotted against frequency for a typical tube, for various orders M of approximation. Results for approximations Y_θ^M to Y_θ are similar. Optimization techniques have been treated previously, and are not the subject of this article; the key point is that the optimization can be performed in such a way that the circuit element values are non-negative, the attribute of passivity may be maintained under truncation.

E. A time-domain system

From the circuit representations in Fig. 4, one may arrive at a corresponding PDE (partial differential equation) system approximating (1) in the time domain. Beginning from system (8), the time domain form may be given, in terms of pressure $p(t, x)$ and particle velocity $v(t, x)$, for time t as

$$\partial_x p + \rho \partial_t v + \Delta = 0, \quad \partial_x (Sv) + \frac{S}{\rho c^2} \partial_t p + Sm = 0. \tag{12}$$

The terms $\Delta(t, x)$ and $m(t, x)$ are due to viscous and thermal effects, respectively, and can be interpreted as the voltage and current across the one-port circuit elements shown in Fig. 4. Using Kirchhoff's connection laws, one may write for Δ, with reference to Fig. 4:

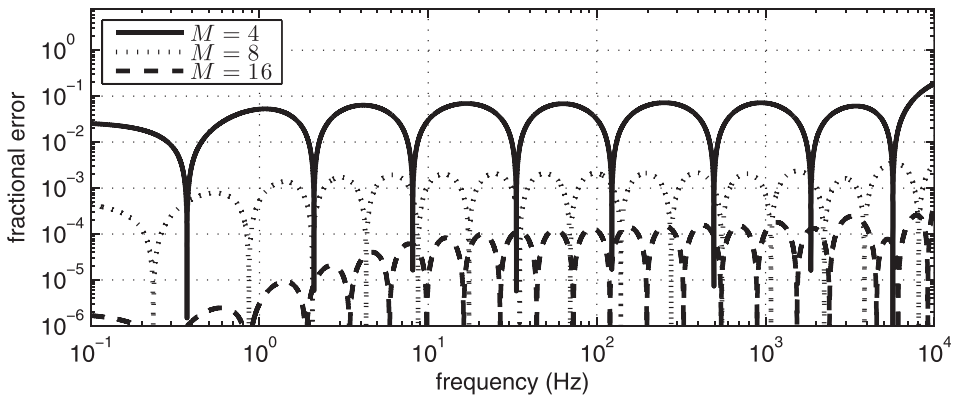

FIG. 5. Fractional error in the real part of approximations Z_v^M to Z_v, as a function of frequency in Hz, for $M = 4$, 8, and 16. The tube is of radius 7.5 mm, and optimization over the range of frequencies from 0.1 to 10 000 Hz.

$$\Delta = \sum_{q=0}^{M} \Delta_q, \quad v = v_q + v'_q, \quad q = 1, \ldots, M, \tag{13}$$

where Δ_q has the interpretation of a partial voltage, and v_q and v'_q of partial currents. Using the definitions of the circuit elements,

$$\Delta_0 = R_0 v, \quad \Delta_q = R_q v_q = L_q \partial_t v'_q, \quad q = 1, \ldots, M. \tag{14}$$

Similarly, for m, Kirchhoff's laws give

$$p = p_0 + \tilde{p}, \quad m = \sum_{q=0}^{M} m_q, \quad \tilde{p} = \tilde{p}_q + \tilde{p}'_q, \quad q = 1 \ldots, M, \tag{15}$$

where p_0, $\tilde{p}_q$ and $\tilde{p}'_q$ have the interpretations of partial voltages, and m_q of partial currents. Again using the definitions of the circuit elements,

$$m = C_0 \partial_t p_0, \quad m_0 = G_0 \tilde{p}, \tag{16a}$$

$$m_q = G_q \tilde{p}_q = C_q \partial_t \tilde{p}'_q, \quad q = 1, \ldots, M. \tag{16b}$$

The boundary conditions (5) may be transferred directly from the frequency domain as

$$v(t, 0) = v_{in}(t), \quad p(t, L) = 0. \tag{17}$$

System (12), accompanied by (13)–(16) is a complete system approximating viscothermal wave propagation in a tube of variable cross section.

F. Energy balance

The approximation presented in Sec. II C is passive, provided that all circuit element values are non-negative. Though obvious from the circuit forms given in Fig. 4, it is useful to illustrate the energy balance directly.

Beginning from the time domain system (12), one may multiply the first equation by Sv, and the second by p; after integrating over the domain $\mathcal{D}$, and summing, the following balance results:

$$d\mathcal{E}_0/dt + \mathcal{B} + \underbrace{\int_{\mathcal{D}} Sv\Delta \, dx}_{\mathcal{W}_v} + \underbrace{\int_{\mathcal{D}} Spm \, dx}_{\mathcal{W}_\theta} = 0. \tag{18}$$

Here,

$$\mathcal{E}_0 = \int_{\mathcal{D}} \frac{\rho S v^2}{2} + \frac{S p^2}{2\rho c^2} \, dx, \quad \mathcal{B} = pSv\big|_0^L, \tag{19}$$

represent the total energy stored in the acoustic field, under lossless conditions and the power supplied at the tube boundaries, respectively. The terms $\mathcal{W}_v$ and $\mathcal{W}_\theta$ in (18) result from viscous and thermal effects, respectively.

For the first such term, using (13),

$$\mathcal{W}_v = \sum_{q=0}^{M} \int_{\mathcal{D}} Sv\Delta_q \, dx \tag{20}$$

$$= \int_{\mathcal{D}} Sv\Delta_0 \, dx + \sum_{q=1}^{M} \int_{\mathcal{D}} S(v_q + v'_q)\Delta_q \, dx, \tag{21}$$

and, using (14), can be decomposed as

$$\mathcal{W}_v = \mathcal{Q}_v + d\mathcal{E}_v/dt, \tag{22}$$

where

$$\mathcal{E}_v = \sum_{q=1}^{M} \frac{1}{2} \int_{\mathcal{D}} SL_q \left(v'_q\right)^2 dx, \tag{23}$$

$$\mathcal{Q}_v = \int_{\mathcal{D}} SR_0 v^2 \, dx + \sum_{q=1}^{M} \int_{\mathcal{D}} SR_q v_q^2 \, dx. \tag{24}$$

Similarly, for W_θ, one may write

$$\mathcal{W}_\theta = \mathcal{Q}_\theta + d\mathcal{E}_\theta/dt, \tag{25}$$

where

$$\mathcal{E}_\theta = \frac{1}{2} \int_{\mathcal{D}} SC_0 p_0^2 \, dx + \sum_{q=1}^{M} \frac{1}{2} \int_{\mathcal{D}} SC_q \left(\tilde{p}'_q\right)^2 dx, \tag{26}$$

$$\mathcal{Q}_\theta = \int_{\mathcal{D}} SG_0 \tilde{p}^2 \, dx + \sum_{q=1}^{M} \int_{\mathcal{D}} SG_q \tilde{p}_q^2 \, dx. \tag{27}$$

Equation (18) can then be written as the energy balance

$$d\mathcal{E}/dt + \mathcal{B} + \mathcal{Q} = 0, \tag{28}$$

where

$$\mathcal{E} = \mathcal{E}_0 + \mathcal{E}_v + \mathcal{E}_\theta \geq 0, \quad \mathcal{Q} = \mathcal{Q}_v + \mathcal{Q}_\theta \geq 0. \tag{29}$$

The non-negativity of $\mathcal{E}$ and $\mathcal{Q}$ follows directly from the definitions of the constituent terms. Under unforced conditions ($\mathcal{B} = 0$), the energy must be monotonically decreasing over time, i.e.,

$$\mathcal{E}(0) \geq \mathcal{E}(t) \geq 0. \tag{30}$$

$\mathcal{E}(t)$ is then a Lyapunov function for the system as a whole, allowing for bounds on variation of the state itself.

The energy balance property can be transferred to discrete time, in which case it can be used as a means of numerical stability analysis. Such a balance follows from any passive circuit representation, and not merely the Foster forms shown in Fig. 4—the Cauer form given by Thompson *et al.*[15] would give a similar balance. Even more generally, one could make use of any rational positive real approximations to Z_v and Y_θ, though the circuit realisation is an invaluable tool and, as will be seen in Sec. V, can inform numerical design.

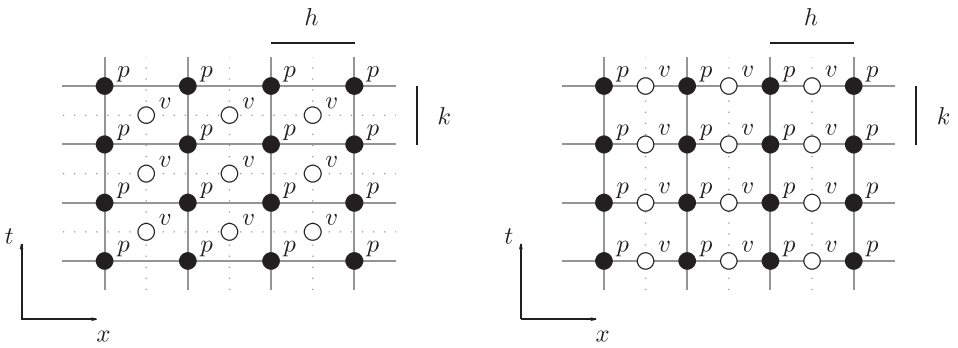

FIG. 6. (Left) Fully interleaved grid. (Right) Spatially interleaved grid.

III. FINITE DIFFERENCE TIME DOMAIN SCHEMES: DEFINITIONS

Time domain numerical schemes operating over regular grids have a long history, dating back at least to the work of Courant *et al.*[26] More modern forms, particularly when used in an interleaved manner (as is the case here) were popularized in the electromagnetic simulation community by Yee,[27] and are often referred to as the finite difference time domain method (FDTD). They have also seen extensive application in acoustics, and have been applied in the case of wave propagation in acoustic tubes by one of the present authors.[11] More recently, time-domain methods incorporating viscothermal effects, in the case of unidirectional wave propagation in acoustic tubes, have been presented by Richoux *et al.*[28] —note that such a representation is not equivalent to that presented here, in that it does not reduce to Webster's equation when losses are not present, and in the case of variable cross section.

A. Grid functions and inner products

For the spatial domain $\mathcal{D} = [0, L]$, define a grid spacing h. For simplicity, assume that h divides the length L evenly, so that there is an integer N such that $N = L/h$. The discrete domain $\bar{d} = [0, \ldots, N]$ represents a set of grid locations, corresponding to the spatial locations $x = lh$, for $l \in \bar{d}$. For finite difference time domain schemes, it is also of interest to define a spatially interleaved domain $d = [0, \ldots, N-1]$, corresponding to the spatial locations $x = \left(l + \frac{1}{2}\right)h$, $l \in d$. Similarly, time may be discretized with a time step k, and indexed by non-negative integer values $\mathbb{Z}^+ = [0, 1, \ldots]$. For time-interleaved schemes, these indices may correspond to the set of time instants $t = nk$, or $t = \left(n + \frac{1}{2}\right)k$, where $n \in \mathbb{Z}^+$ in either case.

In this article, it is mainly fully interleaved approximations that will be of interest, and thus one will employ grid functions p_l^n, to represent approximations to the pressure field $p(x, t)$, for $x = lh$, $l \in \bar{d}$, and $t = nk$, $n \in \mathbb{Z}^+$, and the interleaved grid function $v_{l+1/2}^{n+1/2}$, representing an approximation to the velocity $v(x, t)$, for $x = \left(l + \frac{1}{2}\right)h$, $l \in d$, and $t = \left(n + \frac{1}{2}\right)k$, $n \in \mathbb{Z}^+$ [see Fig. 6(left)]. For the sake of illustration (see Sec. IV), it is also useful to define approximations $v_{l+1/2}^n$ to the velocity which are collocated in time with pressure approximations p_l^n [see Fig. 6(right)].

Consider two grid functions f_l and g_l, defined for $l \in \bar{d}$, and each consisting of $N+1$ real values (the time index is immaterial, and is suppressed here). An l_2 spatial inner product may be defined as

$$\langle f, g \rangle_{\bar{d}} = \frac{h}{2} f_0 g_0 + \sum_{l=1}^{N-1} h f_l g_l + \frac{h}{2} f_N g_N. \tag{31}$$

The factor of $\frac{1}{2}$ applied at the domain endpoints reflects the halving of the effective range covered by a grid point at a boundary.

For two grid functions $f_{l+1/2}$ and $g_{l+1/2}$ defined over $l \in d$, an inner product may be defined as

$$\langle f, g \rangle_d = \sum_{l=0}^{N-1} h f_{l+1/2} g_{l+1/2}. \tag{32}$$

In either case, an l_2 norm may be defined as

$$\|f\| = \sqrt{\langle f, f \rangle}. \tag{33}$$

B. Discrete operators

For a grid function f_l^n, time shift operators e_{t+} and e_{t-} are defined by

$$e_{t+} f_l^n = f_l^{n+1}, \quad e_{t-} f_l^n = f_l^{n-1}. \tag{34}$$

Forward and backward approximations to a first time derivative are defined, in terms of these basic shifts, as

$$\delta_{t+} = \frac{1}{k}(e_{t+} - 1), \quad \delta_{t-} = \frac{1}{k}(1 - e_{t-}), \tag{35}$$

and similarly, forward and backward averaging operations may be defined as

$$\mu_{t+} = \frac{1}{2}(e_{t+} + 1), \quad \mu_{t-} = \frac{1}{2}(1 + e_{t-}). \tag{36}$$

Centered difference and averaging operations may be defined, through operator composition, as

$$\delta_{to} = \mu_{t+} \delta_{t-}, \quad \mu_{to} = \mu_{t+} \mu_{t-}. \tag{37}$$

Similarly, spatial shift, difference and averaging operators may be defined as

$$e_{x+} f_l^n = f_{l+1}^n, \quad e_{x-} f_l^n = f_{l-1}^n, \tag{38}$$

$$\delta_{x+} = \frac{1}{h}(e_{x+} - 1), \quad \delta_{x-} = \frac{1}{h}(1 - e_{x-}), \tag{39}$$

$$\mu_{x+} = \frac{1}{2}(e_{x+} + 1), \quad \mu_{x-} = \frac{1}{2}(1 + e_{x-}). \tag{40}$$

Though applied above in the case of a grid function f_l^n, for integer l and n, all definitions continue to hold for interleaved grid functions such as $f_{l+1/2}^{n+1/2}$.

C. Identities and inequalities

For any l_2 inner product, the following identities hold:

$$\delta_{t+}\left(\frac{1}{2}\|f\|^2\right) = \langle \mu_{t+} f, \delta_{t+} f\rangle, \tag{41a}$$

$$\delta_{t+}\left(\frac{1}{2}\langle f, e_{t-} f\rangle\right) = \langle f, \delta_{to} f\rangle. \tag{41b}$$

An important identity is summation by parts. For a grid function f_l, for $l \in \bar{d}$, and $g_{l+1/2}$, for $l \in d$,

$$\langle f, \delta_{x-} g\rangle_{\bar{d}} = -\langle \delta_{x+} f, g\rangle_d + f_N \mu_{x+} g_{N-1/2} - f_0 \mu_{x-} g_{1/2}. \tag{42}$$

The following identity and inequality hold, for any grid function f:

$$\langle f, e_{t-} f\rangle = \|\mu_{t-} f\|^2 - \frac{k^2}{4}\|\delta_{t-} f\|^2 \geq -\frac{k^2}{4}\|\delta_{t-} f\|^2. \tag{43}$$

Furthermore, the following identity holds, for any grid function f:

$$\langle f, \mu_{to} f\rangle = \mu_{t-}\|\mu_{t+} f\|^2 - \frac{k^2}{8}\delta_{tt}\|f\|^2. \tag{44}$$

For grid functions f_l, $l \in \bar{d}$, and $g_{l+1/2}$, $l \in d$, the following bound holds:

$$\|\sqrt{g}\delta_{x+} f\|_d \leq \frac{2}{h}\|\sqrt{\mu_{x-} g} f\|_{\bar{d}}, \tag{45}$$

where at the domain endpoints, $\mu_{x-} g_{1/2}$ is defined as $g_{1/2}$, and similarly $\mu_{x-} g_{N+1/2}$ is defined as $g_{N-1/2}$.

IV. INTERLEAVED AND NON-INTERLEAVED SCHEMES

There are many approaches to the design of time domain numerical methods. Before presenting a scheme for the full system (12), it is worth pointing out some properties of typical basic schemes in the simplified case of a lossless tube, with constant cross sectional area $S(x) = S_0$. In the absence of viscothermal effects, the system is as defined by (12) with $m = \Delta = 0$. Schemes for this system differ considerably in terms of accuracy, computational cost, as well as stability properties. In particular, it is worth comparing a standard explicit scheme, which is the simplest possible design, and which also has the property of being exact, with a typical implicit scheme. The implicit scheme corresponds to time integration through the trapezoid rule, which is a commonly used technique, particularly in schemes based on the maintenance of an energy-like quantity (e.g., see Jog and Nandy[29]).

A. An explicit scheme

First consider a time-interleaved scheme, which can be written, using operator notation, as

$$\frac{S_0}{\rho c^2}\delta_{t+} p + S_0 \delta_{x-} v = 0, \quad \rho \delta_{t-} v + \delta_{x+} p = 0, \tag{46}$$

where here, $p = p_l^n$ and is defined for $l \in \bar{d}$, and $v = v_{l+1/2}^{n+1/2}$ for $l \in d$. This scheme is explicit (that is, no linear system solutions are required in order to advance the scheme) and the update can be written in full as

$$v_{l+1/2}^{n+1/2} = v_{l+1/2}^{n-1/2} - \frac{k}{\rho h}\left(p_{l+1}^n - p_l^n\right), \tag{47a}$$

$$p_l^{n+1} = p_l^n - \frac{k\rho c^2}{h}\left(v_{l+1/2}^{n+1/2} - v_{l-1/2}^{n+1/2}\right). \tag{47b}$$

The update above can be completed by specifying numerical boundary conditions for the update (47b) at grid points $l = 0$ and $l = N$; these will be given shortly.

In order to obtain a numerical stability condition for scheme (46), energy analysis is an invaluable tool. To this end, one may multiply the first of (46) by $\mu_{t+} p$, and take inner product over the domain $\bar{d}$ to give

$$\frac{S_0}{\rho c^2}\langle \mu_{t+} p, \delta_{t+} p\rangle_{\bar{d}} + S_0 \langle \mu_{t+} p, \delta_{x-} v\rangle_{\bar{d}} = 0. \tag{48}$$

Employing summation by parts (42), the second of (46), as well as the definition of δ_{to} from (37) leads to

$$\frac{S_0}{\rho c^2}\langle \mu_{t+} p, \delta_{t+} p\rangle_{\bar{d}} + \rho S_0 \langle \delta_{to} v, v\rangle_d + \mathfrak{b} = 0, \tag{49}$$

where $\mathfrak{b}$, representing power supplied at the tube endpoints, is defined by

$$\mathfrak{b} = S_0 \mu_{t+} p_N^n \mu_{x+} v_{N-1/2}^{n+1/2} - S_0 \mu_{t+} p_0^n \mu_{x-} v_{1/2}^{n+1/2}. \tag{50}$$

This leads, finally, using identities (41), to the following discrete energy balance:

$$\delta_{t+}\mathfrak{e}_0 + \mathfrak{b} = 0, \tag{51}$$

where the stored numerical energy, or discrete Hamiltonian, is defined by

$$\mathfrak{e}_0 = \frac{S_0}{2\rho c^2}\|p\|_{\bar{d}}^2 + \frac{S_0 \rho}{2}\langle v, e_{t-} v\rangle_d. \tag{52}$$

In order to arrive at a numerical stability condition for this scheme, it is necessary to find a condition under which the numerical stored energy is non-negative. To this end, using the bounds (43) and (45), one may write

$$\begin{aligned}\langle v, e_{t-} v\rangle_d &\geq -\frac{k^2}{4}\|\delta_{t-} v\|_d^2 = -\frac{k^2}{4\rho^2}\|\delta_{x+} p\|_d^2 \\ &\geq -\frac{k^2}{\rho^2 h^2}\|p\|_{\bar{d}}^2,\end{aligned} \tag{53}$$

and thus

$$\mathfrak{e}_0 \geq \frac{S_0}{2\rho c^2}(1 - \lambda^2)\|p\|_{\bar{d}}^2, \quad \lambda = \frac{ck}{h}. \tag{54}$$

The dimensionless constant λ is often referred to as the Courant number.[30] Clearly, the condition for non-negativity of the stored energy is

$$\lambda \leq 1, \tag{55}$$

which is often referred to as the Courant-Friedrichs-Lewy condition. Thus the scheme (46) is conditionally stable.

The scheme (46) is not complete until boundary conditions have been specified. The choices

$$\mu_{x-} v_{1/2}^{n+1/2} = v_{in}^{n+1/2}, \quad p_N^n = 0, \tag{56}$$

correspond to the simple boundary conditions given in (17), and thus the boundary term $\mathfrak{b}$ given in (50) is equal to $-S_0 \mu_{t+} p_0^n v_{in}^{n+1/2}$ and has the interpretation of the negative of power input at the driving end of the tube.

B. An implicit scheme

Consider the following implicit scheme for the system (12) under lossless conditions:

$$\frac{S_0}{\rho c^2} \delta_{t+} p + S_0 \delta_{x-} \mu_{t+} v = 0, \quad \rho \delta_{t+} v + \delta_{x+} \mu_{t+} p = 0. \tag{57}$$

Here, the grid variables $p = p_l^n$ and $v = v_{l+1/2}^n$ are computed together at each time step n. Indeed, at time step n, the unknown grid values to be computed at time step $n+1$ are linearly coupled, and a linear system solution (sparse and banded) is necessary to advance the scheme.

Energy analysis may be carried out in a manner very similar to the case of the explicit scheme, and indeed, a numerical energy balance of the form (51) results, where now, the discrete Hamiltonian is defined as

$$\mathfrak{e}_0 = \frac{S_0}{2\rho c^2} \|p\|_{\bar{d}}^2 + \frac{S_0 \rho}{2} \|v\|_d^2. \tag{58}$$

The quantity is clearly non-negative, and thus the scheme is unconditionally stable—that is, there is no restriction on the time step k or grid spacing h.

C. Comparison: Input impedances

As a simple comparison of the two schemes for the lossless cylinder in Secs. IV A and IV B, consider a computation of the input impedance $Z_{in}(f)$ of a tube of length $L = 0.3$ m as a function of frequency f in Hz. Under boundary conditions (56), the impedance magnitude is $|Z_{in}(f)| = \rho c^2 / S_0 |\tan(2\pi f L/c)|$ [see Fig. 7(top)].

At middle, the numerical input impedance for the explicit scheme (46) is shown, for the maximal value of the Courant number $\lambda = 1$, and for $\lambda = 0.8$. The time step is $k = 5 \times 10^{-5}$ s in this case. Notice that for $\lambda = 1$, the scheme produces a near perfect match to the impedance magnitude of the model system, and that for $\lambda = 0.8$, some warping of the response is noticeable.

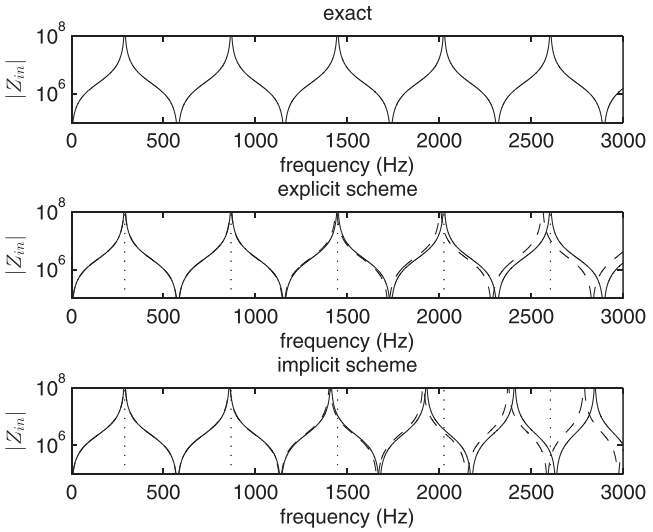

FIG. 7. (Top) Input impedance for a lossless cylindrical tube with an open end. Numerical input impedance for (middle) scheme (46), and (bottom) scheme (57) with $\lambda = 1$ (solid line) and $\lambda = 0.8$ (dashed line), with a time step $k = 5 \times 10^{-5}$ s. Peaks in the impedance curve for the exact solution are shown as dotted lines.

At bottom, the numerical input impedance for the implicit scheme (57) is shown, again for $\lambda = 1$ and $\lambda = 0.8$; in this case, much more severe warping effects are visible.

D. Comment

Both the explicit scheme (46) and the implicit scheme (57) are conservative, with the Hamiltonian as a conserved quantity, though with distinct definitions of the numerical Hamiltonian.

From an analysis perspective, the implicit scheme is clearly much easier to handle, particularly with regard to the determination of numerical stability conditions. Indeed, the scheme presented here can be viewed as resulting from the application of a bilinear transformation; as such, any stable model system [including the full system (12), incorporating viscothermal effects] can be discretized in this manner to yield an unconditionally stable numerical method. Analysis of the explicit scheme is clearly more involved.

On the other hand, the implicit scheme presented here is (a) less accurate than the explicit scheme, and (b) more computationally costly, due to the need for linear system solutions. Thus in practice, there is little advantage to working with implicit schemes, except for the freedom set the time step and grid spacing independently. For this reason, in the remainder of this article, only explicit schemes will be considered. See the concluding remarks in Sec. VII for more comments on this topic.

V. A SCHEME FOR THE COMPLETE SYSTEM

Given the discussion in Sec. IV regarding the merits of time-interleaved schemes, in terms of both accuracy and computational efficiency, it is of interest to examine schemes which approximate the complete system (12)–(16), and which are extensions of (46). Consider the following scheme:

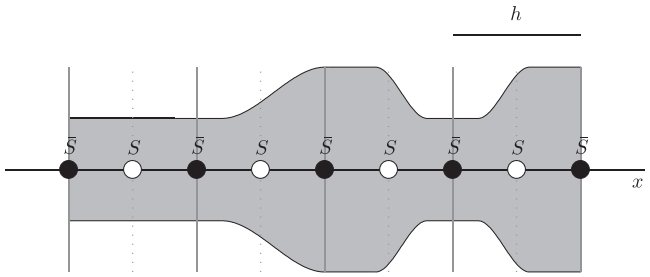

FIG. 8. Spatially interleaved approximations $\bar{S}$ and S to the tube cross-section.

$$\frac{\bar{S}}{\rho c^2}\delta_{t+}p + \delta_{x-}(Sv) + \bar{S}m = 0, \tag{59a}$$

$$\rho\delta_{t-}v + \delta_{x+}p + \Delta = 0. \tag{59b}$$

Here, as for scheme (46), $p = p_l^n$, for $l \in \bar{d}$ and $v = v_{l+1/2}^{n+1/2}$, for $l \in d$ are approximations to the pressure and velocity, respectively. $\bar{S} = \bar{S}_l$, for $l \in \bar{d}$ and $S = S_{l+1/2}$, for $l \in d$ are two spatially-interleaved approximations to the tube cross section (see Fig. 8).

The grid function $\Delta = \Delta_{l+1/2}^n$, for $l \in d$ approximates the voltage-like quantity $\Delta(t,x)$. Introducing partial voltages Δ_q, $q = 1,\ldots,M$, and partial currents v_q and v'_q, $q = 1,\ldots,M$, as in the continuous case in (13), as

$$\Delta = \sum_{q=0}^{N}\Delta_q, \quad v = v_q + v'_q, \quad q = 1,\ldots,M, \tag{60}$$

the circuit elements may be discretized from (14) as

$$\Delta_0 = R_0\mu_{t-}v, \quad \Delta_q = R_q\mu_{t-}v_q = L_q\delta_{t-}v'_q,$$
$$q = 1,\ldots,M. \tag{61}$$

Similarly, the grid function $m_l^{n+1/2}$ approximates the current-like quantity $m(t, x)$. Introduce partial currents and partial voltages, again as in (15), as

$$p = p_0 + \tilde{p}, \quad m = \sum_{q=0}^{M} m_q, \quad \tilde{p} = \tilde{p}_q + \tilde{p}'_q,$$
$$q = 1\ldots,M, \tag{62}$$

and for the definition of circuit elements, from (16), the following discretization:

$$m = C_0\delta_{t+}p_0, \quad m_0 = G_0\mu_{t+}\tilde{p}, \tag{63a}$$

$$m_q = G_q\mu_{t+}\tilde{p}_q = C_q\delta_{t+}\tilde{p}'_q, \quad q = 1,\ldots,M. \tag{63b}$$

The system (59)–(63) is a complete algorithm corresponding to system (12)–(16). The variables Δ_q and m_q, $q = 0,\ldots,M$ may ultimately be eliminated. It admits an explicit implementation, presented in full in Table I.

A. Energy balance

Stability analysis for the scheme given at the beginning of Sec. V proceeds in a manner similar to that of the scheme for the lossless cylinder, as in Sec. IV A, through the determination of a numerical energy balance mirroring (28) for the model system. To this end, take the inner product of (59a) with $\mu_{t+}p$ over $\bar{d}$. After employing summation by parts (42) and identities (41), and (59b), one arrives at the following:

$$\delta_{t+}\mathfrak{e}_0 + \mathfrak{b} + \underbrace{\langle v, S\mu_{t+}\Delta\rangle_d}_{\mathfrak{w}_v} + \underbrace{\langle \mu_{t+}p, \bar{S}m\rangle_{\bar{d}}}_{\mathfrak{w}_\theta} = 0. \tag{64}$$

This is analogous to (18), where $\mathfrak{e}_0$, the stored energy corresponding to the lossless system, and the boundary term $\mathfrak{b}$ are given by

$$\mathfrak{e}_0 = \frac{1}{2\rho c^2}\|\sqrt{\bar{S}}p\|_{\bar{d}}^2 + \frac{\rho}{2}\langle v, Se_{t-}v\rangle_d, \tag{65a}$$

$$\mathfrak{b} = \mu_{t+}p_N\mu_{x+}(Sv)_{N-1/2} - \mu_{t+}p_0\mu_{x-}(Sv)_{1/2}, \tag{65b}$$

TABLE I. Given known values of the grid functions v, and v'_q, $q = 1,\ldots,M$ at time step $n-\frac{1}{2}$, and p, p_0 and $\tilde{p}'_q$, $q = 1,\ldots,M$ at time step n, the updates below are to be carried out in the order ① to ⑤.

Explicit Update Form: Scheme (59)–(63)

Velocity updates and scheme parameters

$$\text{①}\ v_{l+1/2}^{n+1/2} = \alpha_{l+1/2}^{(v)}v_{l+1/2}^{n-1/2} + \beta_{l+1/2}^{(v)}(p_{l+1}^n - p_l^n) + \sum_{q=1}^{M}\alpha_{q,l+1/2}^{(v)}v_{q,l+1/2}^{\prime n-1/2} \quad \text{②}\ v_{q,l+1/2}^{\prime n+1/2} = \tau_{q,l+1/2}^{(v)}v_{q,l+1/2}^{\prime n-1/2} + \xi_{q,l+1/2}^{(v)}(v_{l+1/2}^{n+1/2} + v_{l+1/2}^{n-1/2})$$

$$\bar{R}_{q,l+1/2} = \frac{2L_{q,l+1/2}R_{q,l+1/2}}{2L_{q,l+1/2} + kR_{q,l+1/2}} \quad \bar{R}_{l+1/2} = R_{0,l+1/2} + \sum_{q=1}^{M}\bar{R}_{q,l+1/2}$$

$$\alpha_{l+1/2}^{(v)} = \frac{2\rho - k\bar{R}_{l+1/2}}{2\rho + k\bar{R}_{l+1/2}} \quad \beta_{l+1/2} = -\frac{2k/h}{2\rho + k\bar{R}_{l+1/2}} \quad \alpha_{q,l+1/2}^{(v)} = \frac{2k\bar{R}_{q,l+1/2}}{2\rho + k\bar{R}_{l+1/2}} \quad \tau_{q,l+1/2}^{(v)} = \frac{2L_{q,l+1/2} - kR_{q,l+1/2}}{2L_{q,l+1/2} + kR_{q,l+1/2}} \quad \xi_{q,l+1/2}^{(v)} = \frac{kR_{q,l+1/2}}{2L_{q,l+1/2} + kR_{q,l+1/2}}$$

Pressure updates and scheme parameters

$$\text{③}\ p_l^{n+1} = \alpha_l^{(p)}p_l^n + \beta_l^{(p)}(S_{l+1/2}v_{l+1/2}^{n+1/2} - S_{l-1/2}v_{l-1/2}^{n+1/2}) + \alpha_{0,l}^{(p)}p_{0,l}^n + \sum_{q=1}^{M}\alpha_{q,l}^{(p)}\tilde{p}_{q,l}^{\prime n}$$

$$\text{④}\ p_{0,l}^{n+1} = \epsilon_l^{(p)}p_{0,l}^n + \nu_l^{(p)}(p_l^{n+1} + p_l^n) + \sum_{q=1}^{M}\upsilon_{q,l}^{(p)}\tilde{p}_{q,l}^{\prime n} \quad \text{⑤}\ \tilde{p}_{q,l}^{\prime n+1} = \tau_{q,l}^{(p)}\tilde{p}_{q,l}^{\prime n} + \xi_{q,l}^{(p)}(p_l^{n+1} + p_l^n - p_{0,l}^{n+1} - p_{0,l}^n)$$

$$\bar{G}_{q,l} = \frac{2C_{q,l}G_{q,l}}{2C_{q,l} + kG_{q,l}} \quad \bar{G}_l = G_{0,l} + \sum_{q=1}^{M}\bar{G}_{q,l} \quad E_l = \frac{C_{0,l}\rho c^2 k}{2C_{0,l} + \bar{G}_l k}$$

$$\alpha_l^{(p)} = \frac{1 - E_l\bar{G}_l}{1 + E_l\bar{G}_l} \quad \beta_l^{(p)} = -\frac{\rho c^2 k}{\bar{S}_l h(1 + E_l\bar{G}_l)} \quad \alpha_{0,l}^{(p)} = \frac{2E_l\bar{G}_l}{1 + E_l\bar{G}_l} \quad \alpha_{q,l}^{(p)} = \frac{2E_l\bar{G}_{q,l}}{1 + E_l\bar{G}_l}$$

$$\epsilon_l^{(p)} = \frac{2C_{0,l} - \bar{G}_l k}{2C_{0,l} + \bar{G}_l k} \quad \nu_l^{(p)} = \frac{\bar{G}_l k}{2C_{0,l} + \bar{G}_l k} \quad \upsilon_{q,l}^{(p)} = -\frac{2\bar{G}_{q,l}k}{2C_{0,l} + \bar{G}_l k} \quad \tau_{q,l}^{(p)} = \frac{2C_{q,l} - G_{q,l}k}{2C_{q,l} + G_{q,l}k} \quad \xi_{q,l}^{(p)} = \frac{G_{q,l}k}{2C_{q,l} + G_{q,l}k}$$

generalizing the expressions for the case of the cylinder from (52) and (50), respectively. At the tube ends, the values $S_{1/2}$ and $S_{N+1/2}$ are required. These may be set crudely, to the values $S(0)$ and $S(L)$, respectively, or may be extrapolated from the tube profile, provided that the values remain positive.

As in the case of the model system, $\mathfrak{w}_v$ and $\mathfrak{w}_\theta$ correspond to viscous and thermal losses, respectively. From definitions (60)–(63), they may be written as

$$\mathfrak{w}_v = \delta_{t+}\mathfrak{e}_v + \mathfrak{q}_v, \quad \mathfrak{w}_\theta = \delta_{t+}\mathfrak{e}_\theta + \mathfrak{q}_\theta, \tag{66}$$

where

$$\mathfrak{e}_v = \frac{1}{2}\sum_{q=1}^{M} \langle v'_q, SL_q e_{t-} v'_q \rangle_d, \tag{67a}$$

$$\mathfrak{q}_v = \langle v, SR_0\mu_{t0}v\rangle_d + \sum_{q=1}^{M} \langle v_q, SR_q\mu_{t0}v_q\rangle_d, \tag{67b}$$

$$\mathfrak{e}_\theta = \frac{1}{2}\|\sqrt{\bar{S}C_0}p_0\|_{\bar{d}}^2 + \frac{1}{2}\sum_{q=1}^{M}\|\sqrt{\bar{S}C_q}\tilde{p}'_q\|_{\bar{d}}^2, \tag{67c}$$

$$\mathfrak{q}_\theta = \|\sqrt{\bar{S}G_0}\mu_{t+}\tilde{p}\|_{\bar{d}}^2 + \sum_{q=1}^{M}\|\sqrt{\bar{S}G_q}\mu_{t+}\tilde{p}_q\|_{\bar{d}}^2. \tag{67d}$$

A total energy balance for the scheme then follows as

$$\delta_{t+}\mathfrak{e} + \mathfrak{b} + \mathfrak{q} = 0, \tag{68}$$

where the total energy $\mathfrak{e}$ and power loss $\mathfrak{q}$ are given by

$$\mathfrak{e} = \mathfrak{e}_0 + \mathfrak{e}_v + \mathfrak{e}_\theta, \quad \mathfrak{q} = \mathfrak{q}_v + \mathfrak{q}_\theta. \tag{69}$$

B. Modified energy balance and numerical stability

The numerical energy balance in (68), and the constituent terms neatly reflects that of the model system, from (18). In addition, the total energy $\mathfrak{e}$ reduces to that of the lossless cylinder, from (52), when viscothermal losses are not present, and when $S = \bar{S} = S_0$. It does not, however, lead immediately to a numerical stability condition for scheme (59). This can be seen from the form of $\mathfrak{q}_v$ from (67b), which is not necessarily non-negative, as it should be in order to lead to a monotonic decrease in the energy. The choice of an energy function, directly generalizing that of the lossless problem, is thus not a Lyapunov function for this particular numerical method. For a given system, there is not a unique choice of Lyapunov function, and this is particularly true in the present case of lossy systems. Here, we are after an energy function which is (a) non-increasing, implying non-negative power dissipation, and (b) non-negative itself under the condition $\lambda \leq 1$ for the lossless scheme. It is indeed possible to construct modified energy balances which lead to this result, as shown below.

Beginning from the energy balance (68) above, one may find other balances of the form

$$\delta_{t+}\mathfrak{e}_{\text{mod}} + \mathfrak{q}_{\text{mod}} = 0, \tag{70}$$

where

$$\mathfrak{e}_{\text{mod}} = \mathfrak{e} + \mathfrak{e}^\dagger, \quad \mathfrak{q}_{\text{mod}} = \mathfrak{q} + \mathfrak{q}^\dagger, \quad \delta_{t+}\mathfrak{e}^\dagger + \mathfrak{q}^\dagger = 0. \tag{71}$$

A necessary requirement for stability is that $\mathfrak{q}_{\text{mod}} \geq 0$. Beyond this, however, it is clear that because the scheme is explicit, it can only be conditionally stable. An ideal condition, given the discussion in Sec. IV, is that $\mathfrak{e}_{\text{mod}} \geq 0$ when $\lambda \leq 1$; under this condition, the scheme will be stable, and for λ near 1, numerical dispersion will be minimized.

Using identities (43) and (44), the expression for the numerical energy $\mathfrak{e}$ and power loss $\mathfrak{q}$ can be rewritten as

$$\mathfrak{e} = \tilde{\mathfrak{e}}_0 + \tilde{\mathfrak{e}}_v + \mathfrak{e}_\theta - \mathfrak{e}^\dagger, \quad \mathfrak{q} = \tilde{\mathfrak{q}}_v + \mathfrak{q}_\theta - \mathfrak{q}^\dagger, \tag{72}$$

where $\mathfrak{e}_\theta$ and $\mathfrak{q}_\theta$ are as defined in (67), and where the remaining quantities are defined as

$$\tilde{\mathfrak{e}}_0 = \frac{1}{2\rho c^2}\|\sqrt{\bar{S}}p\|_{\bar{d}}^2 + \frac{\rho}{2}\|\sqrt{S}\mu_{t-}v\|_d^2 - \frac{k^2}{8\rho}\|\sqrt{S}\delta_{x+}p\|_d^2, \tag{73a}$$

$$\tilde{\mathfrak{e}}_v = \mu_{t-}\sum_{q=1}^{M}\frac{1}{2}\|\sqrt{SL_q}v'_q\|_d^2 + \frac{k^2}{8\rho}\|\sqrt{S}\Delta\|_d^2, \tag{73b}$$

$$\mathfrak{e}^\dagger = -\frac{k^2}{8}\delta_{t-}\left(\|\sqrt{SR_0}v\|_d^2 + \sum_{q=1}^{M}\|\sqrt{SR_q}v_q\|_d^2\right), \tag{73c}$$

$$\tilde{\mathfrak{q}}_v = \mu_{t+}\left(\|\sqrt{SR_0}\mu_{t-}v\|_d^2 + \sum_{q=1}^{M}\|\sqrt{SR_q}\mu_{t-}v\|_d^2\right), \tag{73d}$$

$$\mathfrak{q}^\dagger = \frac{k^2}{8}\delta_{tt}\left(\|\sqrt{SR_0}v\|_d^2 + \sum_{q=1}^{M}\|\sqrt{SR_q}v\|_d^2\right). \tag{73e}$$

Note, in particular, that $\delta_{t+}\mathfrak{e}^\dagger + \mathfrak{q}^\dagger = 0$, so that the modified energy balance (70) holds, with

$$\mathfrak{e}_{\text{mod}} = \tilde{\mathfrak{e}}_0 + \tilde{\mathfrak{e}}_v + \mathfrak{e}_\theta, \quad \mathfrak{q}_{\text{mod}} = \tilde{\mathfrak{q}}_v + \mathfrak{q}_\theta. \tag{74}$$

From the above, $\mathfrak{q}_{\text{mod}} \geq 0$. For $\mathfrak{e}_{\text{mod}}$, the constituent terms are non-negative, with the exception of $\tilde{\mathfrak{e}}_0$. But, using the inequality (45), one has

$$\tilde{\mathfrak{e}}_0 \geq \frac{1}{2\rho c^2}\|\sqrt{\bar{S}}p\|_{\bar{d}}^2 - \frac{k^2}{2h^2\rho}\|\sqrt{\mu_{x-}\bar{S}}p\|_{\bar{d}}^2. \tag{75}$$

If, furthermore, the interleaved bore approximations S and $\bar{S}$ are related by $\bar{S}_l = \mu_{x-}S_{l+1/2}$, then the condition above reduces to

$$\tilde{\mathfrak{e}}_0 \geq \frac{1}{2\rho c^2}(1-\lambda^2)\|\sqrt{\bar{S}}p\|_{\bar{d}}^2. \tag{76}$$

Thus $\tilde{\mathfrak{e}}_0$, and therefore $\mathfrak{e}_{\text{mod}}$ are non-negative under the CFL condition $\lambda \leq 1$. This serves as the stability condition for scheme (59)–(63). Notice that it is unchanged from the case of the lossless cylinder, from (55). It is important to point out that both $\mathfrak{e}$ and $\mathfrak{e}_{\text{mod}}$ are distinct definitions of the numerical stored energy of the system as a whole, and similarly, $\mathfrak{q}$ and

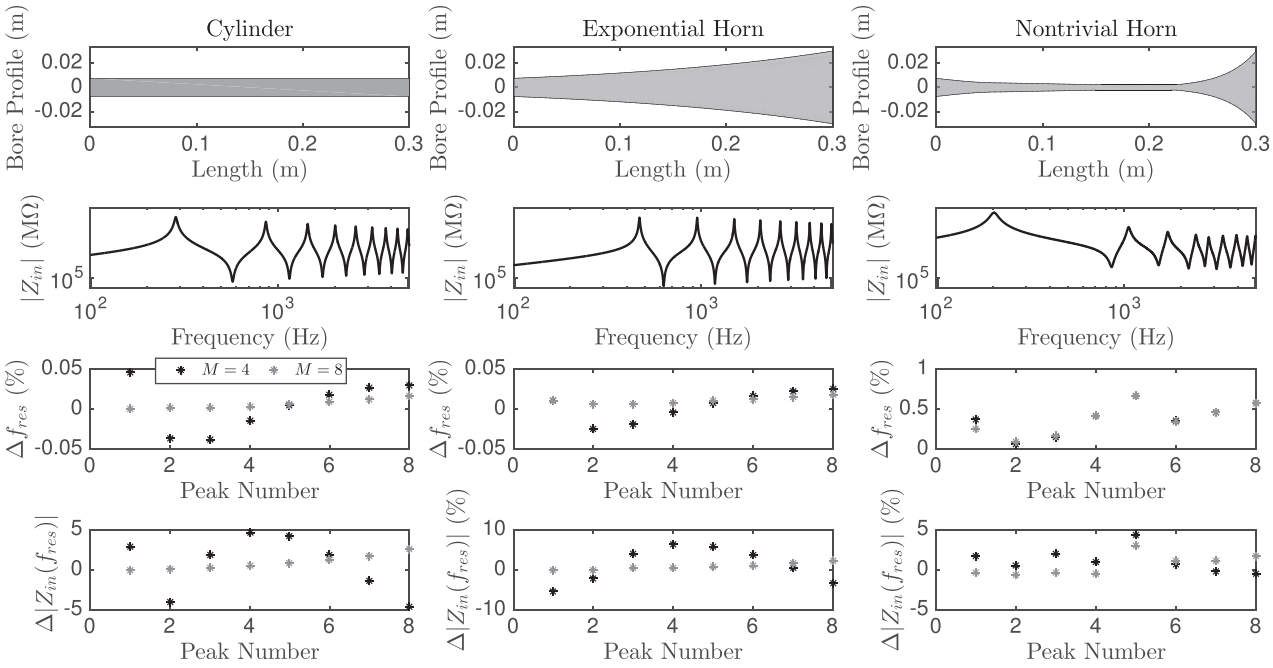

FIG. 9. (Top row) Bore profiles used in the numerical simulations. (Second row) Input impedances calculated using the Transmission Matrix Method that correspond to the profiles above. (Third row) Percentage error of input impedance peak position for the finite-difference scheme compared to the transmission matrix method. (Bottom row) Ratio in dB of the peak magnitude of the finite-difference scheme to the transmission matrix method. Black stars correspond to results for the fourth order structure, grey stars are for the eighth order structure.

$\mathfrak{q}_{\text{mod}}$ are distinct definitions of instantaneous power loss. Both sets of quantities, however, are consistent with the definitions of stored energy and power loss of the model problem in the limit of small time steps (this is easily seen from the dependence of the difference terms $\mathfrak{e}^\dagger$ and $\mathfrak{q}^\dagger$ of k^2).

VI. NUMERICAL RESULTS

In this section, simulation results are presented, using the update equations ①–⑤ in Table I. Three representative cases are considered: a cylinder, an exponential horn, and a horn of nontrivial profile. In all test cases the tube length is $L = 0.3\,\text{m}$ and the opening tube radius is $r_0 = 7.5 \times 10^{-3}\,\text{m}$. The end radii of the exponential and nontrivial horns are 0.03 m. The radius $r(x)$ of the nontrivial horn is given by

$$r(x) = \begin{cases} r_0\left(1 - a_1 \sin\left(\dfrac{\pi x}{2x_1}\right)\right) & : 0 \le x \le x_1 \\ r_0\left(a_1 + \dfrac{a_2 - a_1}{x_2 - x_1}(x - x_1)\right) & : x_1 < x \le x_2 \\ r_0 a_2 & : x_2 < x \le x_3 \\ r_0 a_2 \exp\left(\dfrac{\log(4)}{a_2(L - x_3)}(x - x_3)\right) & : x_3 < x \le L, \end{cases} \tag{77}$$

where $x_1 = 0.06\,\text{m}$, $x_2 = 0.15\,\text{m}$, $x_3 = 0.225\,\text{m}$, $a_1 = 0.5$, and $a_2 = 0.3$ [see Fig. 9(top)].

In all cases, numerically computed input impedances are compared to reference values calculated using the Transmission Matrix Method[3] with a spatial integration step chosen to be $10^{-4}\,\text{m}$ for very high accuracy. These reference impedances are plotted on the middle row of Fig. 9.

Circuit element values are found using the Newton optimization procedure to match the function Z_v over the frequency range 0.1–5000 Hz for a fourth and eighth order circuit structure. Values are obtained for tube radii at increments of $2.5 \times 10^{-3}\,\text{m}$ between 7.5×10^{-3} and $3 \times 10^{-2}\,\text{m}$. Since $\tilde{Y}_\theta$ is of the same form as Z_v, the corresponding values can be reused in the pressure update with appropriate scaling. All numerical simulations are run at a sample rate of 50 kHz over a duration of 10 s. The grid spacing, which must subdivide L evenly, is chosen so that the stability condition (55) is satisfied as close to equality as possible. The pressure equation is excited using $u_{\text{in}}^{n+1/2} = (S_{1/2}v_{1/2}^{n+1/2} + S_{-1/2}v_{-1/2}^{n+1/2})/2$, where u_{in} is a volume velocity source that has a value of unity at $n = 0$ and zero elsewhere. The first eight input impedance peak positions and magnitudes are calculated using a quadratic fit and compared to the reference input impedances. The third row of Fig. 9 shows the percentage error of the peak position and the bottom of Fig. 9 shows the ratio of the magnitude of the peaks.

For the cylinder and the exponential horn the peak position error is less than 0.05% for the fourth order structure and less than 0.02% for the eighth order structure. The nontrivial horn has a peak position error 0.7% for both the fourth and eighth order structures. The larger error for the nontrivial horn results are likely due to the effect of discretizing the domain of a tube with a complex profile. For all test cases, the magnitude ratio is less than 0.3 dB for the fourth order structures and less than 0.15 dB for the eighth order structure.

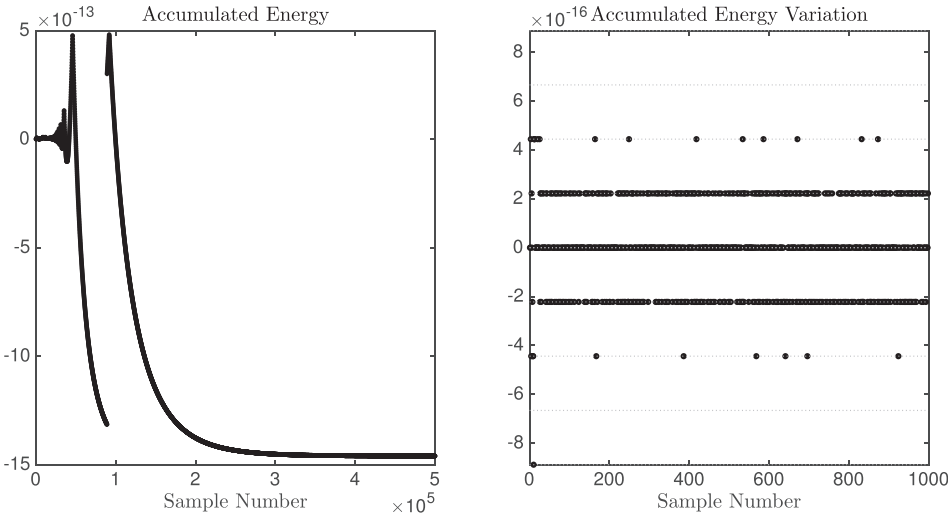

FIG. 10. (Left) Accumulated energy for the nontrivial horn with eighth order circuit structure. (Right) Variation of accumulated energy over the first 1000 time steps (black) and multiples of the machine error (grey).

To check that a numerical energy balance is satisfied, the accumulated energy[31] is introduced and defined as

$$\frac{\mathsf{e}_{\mathrm{mod}}^{n+1} - \mathsf{e}_{\mathrm{mod}}^{0} + k\sum_{0}^{n} \mathsf{q}_{\mathrm{mod}}^{n+1/2}}{\lfloor \mathsf{e}_{\mathrm{mod}}^{0} \rfloor_2}, \tag{78}$$

where $\lfloor \cdot \rfloor_2$ denotes a rounding to the nearest power of two. The accumulated energy should remain zero; however, due to numerical rounding effects, it remains a small, nonzero value. Figure 10(left) shows the accumulated energy for the nontrivial horn with an eighth order circuit structure. This value is of the order 10^{-13}. Note, in particular, that, despite the numerical energy balance, there is still some variation beyond machine precision (on the order of 10^{-16}), leading to some slow, but bounded long-term drift. Such effects are related to finite-precision rounding effects in the manner in which the scheme coefficients are calculated, the order or operations in the scheme update, as well as in the calculation of the numerical energy balance itself. As has been shown recently,[31] such effects tend to be pronounced in systems with a small degree of loss. As yet, a complete explanation is not available. Over shorter timescales, bitwise variation is apparent: at right of Fig. 10 is shown the accumulated energy variation over the first 1000 time steps.

VII. CONCLUDING REMARKS

This article is concerned with design principles for finite difference time-domain modeling for ducts of variable cross-section. An energy-balanced formulation has been used in order to arrive at a stability condition for an explicit scheme, which is unchanged from the case of the lossless tube of uniform cross-section, and is thus convenient to use in practice. Positive real approximations to the viscous and thermal immittances are employed, using designs optimized over target frequency ranges, and with error dependent primarily on the order of the approximation. As has been shown in Sec. VI, errors relative to direct frequency domain calculations of input impedances are small at sample rates which are low relative to the frequency range of interest, and indeed can be made as small as desired through higher-order models of the viscothermal immittances. Another benefit of the immittance approximations described here and similar forms elsewhere[15] is that intermediate high-frequency approximations to the immittances,[3,22] leading to fractional-order PDE systems[9,11] may be avoided, and thus the approximated immittances are valid in both the high- and low-frequency ranges, and without the appearance of a spurious singularity at zero frequency.

It is worth emphasizing that there are many distinct energy-balanced schemes for the model system, each with a distinct definition of numerical energy and power loss; solutions for any such scheme, however, converge to that of the model system under grid or time step refinement, provided it is stable, and numerically consistent with the underlying model problem. There is thus a good degree of freedom in numerical design, which can be exploited in order to arrive at efficient schemes with very high accuracy. The scheme chosen here is explicit and employs a somewhat hybridized design, with distinct discretization rules used for the propagative and lossy parts of the immittances. Other energy-balanced schemes are possible, but there are great differences in terms of performance, as has been illustrated in the case of the lossless uniform tube in Sec. IV. Unconditionally stable implicit schemes for the acoustic tube, though much easier to analyze, are both more computationally costly, and less accurate, with significant dispersion effects, leading to large deviations in the profile of the input impedance curve. In such a formalism, the numerical energy function is usually constrained to be non-negative from the outset; in the method presented here, it is not, leading to the standard Courant-Friedrichs-Lewy stability condition[26] for explicit schemes, now extended to the case of a lossy tube of variable cross section.

The main reason for exploring direct time-stepping methods, as opposed to frequency-domain methods, is to serve as a starting point for numerical designs for the nonlinear system;[32] stability and good accuracy under linear conditions would appear to be a necessary prerequisite for an extension to the nonlinear case. That being said, in the

extension to the nonlinear case, new numerical issues emerge—indeed, it is not known whether a Courant-type condition of the type $\lambda \leq 1$ will remain in force, or if it must be weakened, leading to increased numerical dispersion error. In particular, the technique for showing numerical stability here, that of demonstrating a numerical energy balance, for which both stored energy and dissipated power are non-negative, must be extended to an entropy balance,[33] a well-known technique in the numerical simulation of shocks.[34] There is not, to the knowledge of these authors, an extension of the Zwikker-Kosten model, incorporating boundary layer effects and variable cross-sectional area to the case of nonlinear wave propagation.

ACKNOWLEDGMENTS

This work was supported by the European Research Council, under Grant No. ERC-2011-StG-279068-NESS.

[1]C. Zwikker and C. Kosten, *Sound Absorbing Materials* (Elsevier, New York) (1949), pp. 1–147.
[2]H. Tijdeman, "On the propagation of sound waves in cylindrical tubes," J. Sound Vib. **39**, 1–33 (1975).
[3]R. Caussé, J. Kergomard, and X. Lurton, "Input impedance of brass musical instruments—comparison between experiment and numerical models," J. Acoust. Soc. Am. **75**, 241–254 (1984).
[4]A. Hirschberg, J. Gilbert, R. Msallam, and A. Wijnands, "Shock waves in trombones," J. Acoust. Soc. Am. **99**, 1754–1758 (1996).
[5]K. van den Doel and U. Ascher, "Real-time numerical solution of Webster's equation on a non-uniform grid," IEEE Trans. Audio Speech Language Proc. **16**, 1163–1172 (2008).
[6]J. Martinez and J. Agulló, "Conical bores. part I: Reflection functions associated with discontinuities," J. Acoust. Soc. Am. **84**, 1613–1619 (1988).
[7]A. Barjau, D. Keefe, and S. Cardona, "Time-domain simulation of acoustical waveguides with arbitrarily spaced discontinuities," J. Acoust. Soc. Am. **105**, 1951–1964 (1999).
[8]D. Berners, "Acoustics and Signal processing techniques for physical modelling of brass instruments," Ph.D. thesis, Stanford University, Stanford, CA (1999).
[9]R. Mignot, T. Hélie, and D. Matignon, "Digital waveguide modeling for wind instruments: Building a state space representation based on the Webster Lokshin model," IEEE Trans. Audio Speech Language Proc. **18**, 843–854 (2010).
[10]J. Kelly and C. Lochbaum, "Speech synthesis," in *Proceedings of the Fourth International Congress on Acoustics*, Copenhagen, Denmark (1962), paper G42, pp. 1–4.
[11]S. Bilbao and J. Chick, "Finite difference time domain simulation for the brass instrument bore," J. Acoust. Soc. Am. **134**, 3860–3871 (2013).
[12]E. Hairer and G. Wanner, *Geometric Numerical Integration: Structure-Preserving Algorithms for Ordinary Differential Equations* (Springer, Berlin, Germany, 2006).
[13]J. Chabassier, "Modeling and numerical simulation of the piano through physical modeling," Ph.D. thesis, Ecole Polytechnique, Palaiseau, France (2012).
[14]S. Bilbao, *Numerical Sound Synthesis: Finite Difference Schemes and Simulation in Musical Acoustics* (John Wiley and Sons, Chichester, UK, 2009), 137 pp.
[15]S. Thompson, T. Gabrielson, and D. Warren, "Analog model for thermoviscous propagation in a cylindrical tube," J. Acoust. Soc. Am. **135**, 585–590 (2014).
[16]S. Bilbao, R. Harrison, J. Kergomard, B. Lombard, and C. Vergez, "Passive models of viscothermal wave propagation in acoustic tubes," J. Acoust. Soc. Am. **138**, 555–558 (2015).
[17]T. Hélie, "Unidimensional models of acoustic propagation in axisymmetric waveguides," J. Acoust. Soc. Am. **114**, 2633–2647 (2003).
[18]A. Benade, "On the propagation of sound waves in a cylindrical conduit," J. Acoust. Soc. Am. **44**, 616–623 (1968).
[19]F. Silva, P. Guillemain, J. Kergomard, B. Mallaroni, and A. Norris, "Approximation forms for the acoustic radiation impedance of a cylindrical pipe," J. Sound Vib. **322**, 255–263 (2009).
[20]A. Webster, "Acoustical impedance, and the theory of horns and of the phonograph," Proc. Natl. Acad. Sci. U.S.A. **5**, 275–282 (1919).
[21]L. Weinberg, *Network Analysis and Synthesis* (R. E. Kreiger, New York, 1975), 312 pp.
[22]D. Keefe, "Acoustical wave propagation in cylindrical ducts: Transmission line parameter approximations for isothermal and nonisothermal boundary conditions," J. Acoust. Soc. Am. **75**, 58–62 (1984).
[23]T. Hélie and D. Matignon, "Diffusive representations for the analysis and simulation of flared acoustic pipes with visco-thermal losses," Math. Models Methods Appl. Sci. **16**, 503–536 (2006).
[24]J. Kergomard, "General equivalent electric circuits for acoustic horns," J. Audio Eng. Soc. **36**, 948–955 (1988).
[25]R. Foster, "A reactance theorem," Bell Syst. Tech. J. **3**, 259–267 (1924).
[26]R. Courant, K. Friedrichs, and H. Lewy, "On the partial differential equations of mathematical physics," Math. Ann. **100**, 32–74 (1928).
[27]K. Yee, "Numerical solution of initial boundary value problems involving Maxwell's equations in isotropic media," IEEE Trans. Ant. Prop. **14**, 302–307 (1966).
[28]O. Richoux, B. Lombard, and J.-F. Mercier, "Generation of acoustic solitary waves in a lattice of Helmholtz resonators," Wave Motion **56**, 85–99 (2015).
[29]C. Jog and A. Nandy, "Conservation properties of the trapezoidal rule in linear time domain analysis of acoustics and structures," J. Vib. Acoust. **137**, 021010 (2015).
[30]B. Gustafsson, H.-O. Kreiss, and J. Oliger, *Time Dependent Problems and Difference Methods* (John Wiley and Sons, New York, 1995).
[31]A. Torin, "Percussion instrument modelling in 3d: Sound synthesis through time domain numerical simulation," Ph.D. thesis, The University of Edinburgh, Edinburgh, United Kingdom (2015).
[32]N. Sugimoto, "Burgers equation with a fractional derivative; hereditary effects on nonlinear acoustic waves," J. Fluid Mech. **225**, 631–653 (1991).
[33]E. Tadmor, "Entropy functions for symmetric systems of conservation laws," J. Math. Anal. Appl. **122**, 355–359 (1987).
[34]E. Tadmor, "Entropy stability theory for difference approximations of nonlinear conservation laws and related time-dependent problems," Acta Num. **12**, 451–512 (2003).